Open access • Journal Article • DOI:10.1116/1.4966198

Aluminum oxide/titanium dioxide nanolaminates grown by atomic layer deposition: Growth and mechanical properties — Source link

Oili Ylivaara, Lauri Kilpi, Xuwen Liu, Sakari Sintonen ...+9 more authors

Institutions: VTT Technical Research Centre of Finland, Aalto University, University of Jyväskylä

Published on: 01 Jan 2017 - Journal of Vacuum Science and Technology (American Vacuum Society (AVS))

Topics: Atomic layer deposition, Thin film, Bilayer, Residual stress and Silicon

Ylivaara, Oili M E; Kilpi, Lauri; Liu, Xuwen; Sintonen, Sakari; Ali, Saima; Laitinen, Mikko; Julin, Jaakko; Haimi, Eero; Sajavaara, Timo; Lipsanen, Harri; Hannula, Simo Pekka; Ronkainen, Helena; Puurunen, Riikka

Aluminum oxide/titanium dioxide nanolaminates grown by atomic layer deposition

Published in:
JOURNAL OF VACUUM SCIENCE AND TECHNOLOGY A

DOI:
10.1116/1.4966198

Published: 01/01/2017

Document Version
Publisher's PDF, also known as Version of record

Please cite the original version:
Ylivaara, O. M. E., Kilpi, L., Liu, X., Sintonen, S., Ali, S., Laitinen, M., Julin, J., Haimi, E., Sajavaara, T., Lipsanen, H., Hannula, S. P., Ronkainen, H., & Puurunen, R. (2017). Aluminum oxide/titanium dioxide nanolaminates grown by atomic layer deposition: Growth and mechanical properties. *JOURNAL OF VACUUM SCIENCE AND TECHNOLOGY A*, *35*(1), 1-13. [01B105]. https://doi.org/10.1116/1.4966198

Aluminum oxide/titanium dioxide nanolaminates grown by atomic layer deposition: Growth and mechanical properties

Oili M. E. Ylivaara, Lauri Kilpi, Xuwen Liu, Sakari Sintonen, Saima Ali, Mikko Laitinen, Jaakko Julin, Eero Haimi, Timo Sajavaara, Harri Lipsanen, Simo-Pekka Hannula, Helena Ronkainen, and Riikka L. Puurunen

Citation: Journal of Vacuum Science & Technology A: Vacuum, Surfaces, and Films **35**, 01B105 (2017); doi: 10.1116/1.4966198

View online: http://dx.doi.org/10.1116/1.4966198

View Table of Contents: http://avs.scitation.org/toc/jva/35/1

Published by the American Vacuum Society

Aluminum oxide/titanium dioxide nanolaminates grown by atomic layer deposition: Growth and mechanical properties

Oili M. E. Ylivaara[a] and Lauri Kilpi
VTT Technical Research Centre of Finland, P.O. Box 1000, FI-02044 VTT, Finland

Xuwen Liu
Department of Materials Science and Engineering, Aalto University School of Chemical Technology, P.O. Box 16200, FI-00076 Aalto, Finland

Sakari Sintonen and Saima Ali
Department of Micro- and Nanosciences, Aalto University School of Electrical Engineering, P.O. Box 13500, FI-00076 Aalto, Finland

Mikko Laitinen and Jaakko Julin
Department of Physics, University of Jyväskylä, P.O. Box 35, FI-40014 Jyväskylä, Finland

Eero Haimi
Department of Materials Science and Engineering, Aalto University School of Chemical Technology, P.O. Box 16200, FI-00076 Aalto, Finland

Timo Sajavaara
Department of Physics, University of Jyväskylä, P.O. Box 35, FI-40014 Jyväskylä, Finland

Harri Lipsanen
Department of Micro- and Nanosciences, Aalto University School of Electrical Engineering, P.O. Box 13500, FI-00076 Aalto, Finland

Simo-Pekka Hannula
Department of Materials Science and Engineering, Aalto University School of Chemical Technology, P.O. Box 16200, FI-00076 Aalto, Finland

Helena Ronkainen and Riikka L. Puurunen
VTT Technical Research Centre of Finland, P.O. Box 1000, FI-02044 VTT, Finland

(Received 4 July 2016; accepted 13 October 2016; published 4 November 2016)

Atomic layer deposition (ALD) is based on self-limiting surface reactions. This and cyclic process enable the growth of conformal thin films with precise thickness control and sharp interfaces. A multilayered thin film, which is nanolaminate, can be grown using ALD with tuneable electrical and optical properties to be exploited, for example, in the microelectromechanical systems. In this work, the tunability of the residual stress, adhesion, and mechanical properties of the ALD nanolaminates composed of aluminum oxide (Al_2O_3) and titanium dioxide (TiO_2) films on silicon were explored as a function of growth temperature (110–300 °C), film thickness (20–300 nm), bilayer thickness (0.1–100 nm), and TiO_2 content (0%–100%). Al_2O_3 was grown from Me_3Al and H_2O, and TiO_2 from $TiCl_4$ and H_2O. According to wafer curvature measurements, Al_2O_3/TiO_2 nanolaminates were under tensile stress; bilayer thickness and growth temperature were the major parameters affecting the stress; the residual stress decreased with increasing bilayer thickness and ALD temperature. Hardness increased with increasing ALD temperature and decreased with increasing TiO_2 fraction. Contact modulus remained approximately stable. The adhesion of the nanolaminate film was good on silicon. © *2016 American Vacuum Society*. [http://dx.doi.org/10.1116/1.4966198]

I. INTRODUCTION

Atomic layer deposition (ALD) is a thin film growth technique developed independently in the 1960s and 1970s under the names molecular layering and atomic layer epitaxy, respectively.[1,2] ALD was industrialized in 1980s for thin-film electroluminescent (TFEL) displays and in 2000s for microelectronics such as dynamic random-access memories and complementary metal-oxide semiconductor transistors.[1–5] ALD thin films can be grown with submonolayer thicknesses, since in each growth cycle, self-limiting surface reactions take place.[3,4,6] This unique feature enables precise thickness control and high conformality[7,8] of the grown film by simply controlling the number of growth cycles.

Nanolaminates are multilayer films, engineered of at least two different materials.[9,10] A typical nanolaminate structure, presented in Fig. 1, is composed of repeated bilayers, each bilayer consisting of two materials with separately defined thicknesses. These individual sublayer thicknesses are determined by the number of ALD growth cycles. To reach the total nanolaminate thickness, the number of bilayers is repeated by a given number of the nanolaminate supercycles. A nanolaminate might also have optional bottom and top layer (a "cap").

[a]Electronic mail: oili.ylivaara@vtt.fi

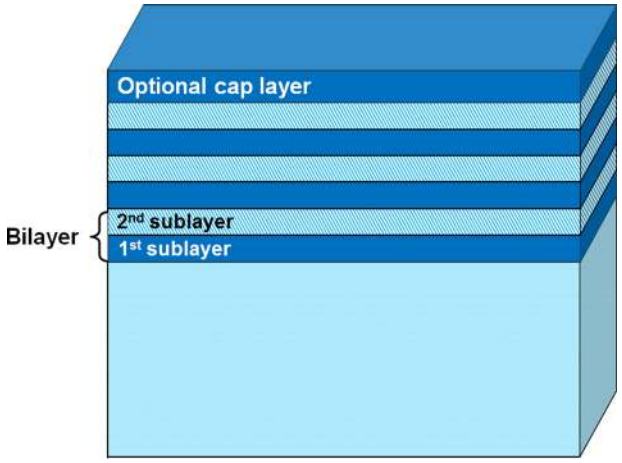

FIG. 1. (Color online) Schematic representation of a typical nanolaminate structure with three bilayers and a cap layer.

The thickness control, multilayer processing capability, uniformity, and conformality of the ALD (Refs. 10–12) are advantageous in processing nanolaminated thin films. With ALD, nanolaminates can be grown either with sharp interfaces[13,14] or gradual composition changes.[15] Thus, the ALD enables engineering of the nanolaminates with tuneable physical properties,[15] by choosing the layer thickness to be less or equal to the length scale that defines the physical property.[6,15,16]

ALD nanolaminates were introduced in TFEL-displays[17,18] and optical dielectric multilayers.[10,11] Especially, Al_2O_3/TiO_2 nanolaminates have applications in optics,[10,19] because the Al_2O_3 is a low-refractive-index and the TiO_2 a high-refractive-index material.[20] In mixed oxides[21] (Al_2O_3 and TiO_2) and Al_2O_3/TiO_2 nanolaminates,[22] tailored optical properties varying from Al_2O_3 to TiO_2 with gradual composition change have been demonstrated. The electrical properties[23,24] can be tuned by adjusting either the TiO_2 fraction[25,26] or the bilayer thickness[27–30] or with an interfacial layers.[31]

The effect of alloying elements on controlling the grain size is well known in bulk materials.[32] In ALD, for example, aluminum oxide is known to prevent or retard the growth of crystallites by preventing the nucleation events,[33,34] thus reducing the surface roughness of the film.[9,12]

Nanolaminates have been reported to have adjustable mechanical properties, such as hardness and elastic modulus.[35–39] They have been reported to adhere to substrates better than some reference films.[40,41] Better corrosion resistance[41–44] and thermal stability[45,46] have also been reported for nanolaminates.

Although ALD Al_2O_3 and TiO_2 have been widely studied both as such and as nanolaminates, little is known on how composition and morphology of the nanolaminate film influence residual stress, adhesion, and mechanical properties. The idea of residual stress adjustment has been introduced in Al_2O_3/TiO_2 multilayer materials already in 2005,[47] and since then scattered residual stress data have been published, for example, as a function of nanolaminate thickness for films grown at 100 °C,[48] and for nanolaminates and mixed oxides grown at 220 °C.[49] The mechanical properties such as elastic modulus and hardness have been studied as a function of bilayer thickness using nanoindentation for films grown at 200 °C (Ref. 39) and elastic modulus by bulge and shaft loading test.[49] The Al_2O_3/TiO_2 nanolaminate adhesion has been studied by indentation on the stainless steel substrate,[40,41] and for reference ALD Al_2O_3 and ALD TiO_2 materials on silicon[50] and on polymeric substrate.[51] Since there is no systematic data on residual stress, the adhesion and mechanical properties of Al_2O_3/TiO_2 nanolaminates on silicon as a function of ALD temperature, total film thickness, bilayer thickness, and TiO_2 fraction, the purpose of this work was to accumulate this knowledge. Another related publication continues on the same samples, reporting on the thermal conductivity of Al_2O_3/TiO_2 layers.[52]

II. EXPERIMENT

A. Sample preparation

The ALD nanolaminates composed of sequential Al_2O_3 and TiO_2 layers (later called ATO nanolaminates) and reference Al_2O_3 and TiO_2 films were grown in a top-flow Picosun™ R-150 ALD reactor with three reactant lines. The precursors were trimethylaluminum (Me_3Al), titanium tetrachloride ($TiCl_4$), and deionized water. Nitrogen (purity > 99.999%) was used both as a purge gas and for flushing the reactant lines with a constant 200 sccm flow. The electronic grade Me_3Al and $TiCl_4$ precursors were purchased from SAFC Hitech. The Me_3Al and $TiCl_4$ precursor bubblers were cooled with a Peltier element to about 17 and 14 °C, respectively. Water was used at room temperature without cooling. The precursor dose and purge times were 0.1 and 4.0 s, respectively, for Me_3Al, $TiCl_4$, and H_2O.

ALD films were grown on 380 ± 5 μm thick double side polished and 675 ± 15 μm thick single side polished 150 mm, p-type (100) silicon wafers from Okmetic Oyj. Before the film growth, the silicon wafers were cleaned using Radio Corporation of America (RCA)-cleaning [SC-1 (NH_3:H_2O_2:H_2O), hydrofluoric acid-dip (1%), and SC-2 (HCl:H_2O_2:H_2O) as described in Ref. 53], covering the wafers with a chemical oxide.

For the reference Al_2O_3 (Ref. 53) and TiO_2 (some of the results from Ref. 54) films, the growth temperature was varied from 110 to 300 °C while the total thickness was kept constant at about 100 nm. The "standard" ATO nanolaminate with 60% of TiO_2 was grown at 200 °C, targeting for 5 nm bilayer thickness, composed of 2 nm Al_2O_3 and 3 nm TiO_2 sublayers.[55] The nanolaminate structure started with the growth of an Al_2O_3 layer followed by growth of TiO_2. There was no bottom layer in the nanolaminate, except for the chemical oxide formed during the cleaning sequence. The nanolaminate structure was capped with about 2 nm of Al_2O_3. Al_2O_3 capping was used similarly as in the nanolaminate test series of 2009.[55] Four different sample sets were designed and fabricated, where one parameter at a time was varied: (1) the growth temperature from 110 to 300 °C, (2) the TiO_2 fraction from 0% to 100%, (3) the nominal bilayer thickness from 0.1 to 100 nm, and (4) the nanolaminate thickness from 20 to 300 nm. The amount of cycles needed to grow the laminate structure with a desired target thickness

was calculated from the growth per cycle (GPC) values of the reference Al_2O_3 and TiO_2 samples grown in 700 and 1400 cycles, respectively, with measured thicknesses of 53.4, 60.6, 67.3, 67.5, and 63.1 nm for Al_2O_3 and 70.4, 58.4, 55.2, 72.5, and 67.2 nm for TiO_2 grown at temperatures 110, 150, 200, 250, and 300 °C, respectively. Linearly increasing thickness was assumed for the ATO nanolaminate when the experiments were designed.

B. Characterization

The thickness and refractive index was analyzed with spectroscopic reflectometry FilmTek 4000 using wavelength range of 400–1600 nm. Refractive index was reported for 633 nm wavelength. The thickness and density were analyzed with x-ray reflectivity (XRR), and the crystallinity was studied by using grazing incidence x-ray diffractometry (GIXRD) as described in Ref. 14. Both the XRR and the GIXRD measurements were performed using a Philips X'Pert Pro diffractometer with parallel beam conditions, and x-ray wavelength, acceleration voltage and anode current Cu-K_α, 40 kV and 40 mA, respectively. The thickness and density values were determined by simulating XRR curves with the software X'PERT REFLECTIVITY.

The film composition and impurities were analyzed with the time-of flight elastic recoil detection analysis (TOF-ERDA)[56] and Rutherford backscattering spectrometry (RBS) using 2 MeV He-beam.

The residual stress of the ALD films on silicon was determined with surface profilometry Veeco Dektak V200-Si and wafer curvature method using Stoney's equation as described in Ref. 53. The wafers were scanned parallel and perpendicular to the wafer flat using a 120 mm scan length. The wafer curvature was also measured with TOHO FLX-2320-S to acquire thermal properties by *in situ* heating the as-grown wafers. The measurement started maximum 30 min after taking the wafer from the ALD tool and were conducted under continuous nitrogen flow from room temperature up to 500 °C. The measurement was repeated three times consecutively. The scan length was 120 mm, and the measurement direction was parallel to the wafer flat. The residual stress values are given with the maximum measurement uncertainty, as calculated in Ref. 53, taking into account the uncertainty in the film and the substrate thicknesses in addition to the wafer curvature measurement.

Scratch testing was carried out to evaluate the adhesion performance of the ALD film using a CSM Micro-Combi tester. A Rockwell C diamond tip with a radius of 20 μm was used in scratch testing with increasing scratch force from 0.05 to 1.3 N and loading rate of 4.17 N/min. The scratch length was 3.0 mm, and three scratches per sample were carried out. Four critical loads for adhesion were determined as described in Ref. 50, namely, L_{CSi1}, L_{CSi2}, L_{CALD1}, and L_{CALD2} representing the critical loads for the silicon substrate failure and the film delamination.

The mechanical behavior of the ATO nanolaminates was studied by nanoindentation using a TriboIndenter® TI-900 (Hysitron, Inc.) nanomechanical testing system, fine-tuned to eliminate the mechanical, acoustic, and electric noise as described in detail in Refs. 53 and 57 for ALD Al_2O_3 films. The instrument was inside a semiclean room under constant laminar airflow to minimize the possible thermal drift during the measurement. Five indents were performed under displacement-control at three preselected depths (40, 60, and 80 nm). The segment time at loading, peak-depth holding and unloading was set as 10, 5, and 5 s, respectively. Here, the contact modulus, which reflects the elastic response of the whole system, including the sample, the indenter, as well as the load frame, is reported. The instrument stability and indentation repeatability were monitored by repeatedly performing a series of 25 indents into a piece of Si wafer during the measurement period.

III. RESULTS

A. Thin film characterization

1. Al_2O_3, TiO_2, and ATO temperature series

The thickness, refractive index, density, crystalline structure, and chemical composition of ATO nanolaminates and reference ALD Al_2O_3 and TiO_2 films were characterized at a temperature range from 110 to 300 °C (Al_2O_3 from Ref. 53 and some of the TiO_2 and ATO characterization results from Refs. 54 and 14, respectively). The results are presented in Table I. The target thickness for total ATO nanolaminate, reference Al_2O_3 and TiO_2 films was 100 nm, while the target thicknesses for the Al_2O_3 and TiO_2 sublayers were 2 and 3 nm, respectively, targeting for 60% TiO_2 fraction and 5 nm bilayer thickness, throughout the temperature range. The GPC values were calculated by dividing the sublayer thicknesses measured by XRR with the number of growth cycles.

The GPC for Al_2O_3 sublayer followed approximately the same trend as a function of ALD temperature as reference ALD Al_2O_3 (Ref. 53) where the GPC increased with increasing ALD temperature until 250 °C after it decreased. For the TiO_2 sublayer, the GPC decreased with increasing ALD temperature. The same GPC trend was observed for the reference ALD TiO_2 at temperature range from 110 to 200 °C. After this, an abrupt rise in GPC was detected, the GPC being approximately at 0.02 nm higher for reference TiO_2 than ATO TiO_2 sublayer at 250 and 300 °C. The total ATO nanolaminate thickness (Table II) was approximately constant at the temperature range from 110 to 200 °C, after which thinner films were measured, and the measured thickness deviated from the targeted 100 nm thickness for films grown at 250 and 300 °C. The reflectometry measurements and total thicknesses calculated from XRR sublayer thicknesses were in line. The film nonuniformity (1σ) was about 2.0% for films grown at 110 to 200 °C and improved to 1.1% for film grown at 300 °C.

The refractive index of the nanolaminate was expected to slightly increase with increasing ALD temperature on the basis of the results from the reference Al_2O_3 and TiO_2, presented in Table I. According to the reflectometry measurements, refractive index reached a maximum value at 200 °C and thereafter decreased. The main reason was that the

TABLE I. Thin film characterization results as a function of the growth temperature for ALD Al_2O_3, TiO_2, and ATO nanolaminates. The pulse sequence for the growth was (0.1–4.0) s for pulse and purge of TMA, $TiCl_4$, and H_2O. The GPC values, for reference Al_2O_3 and TiO_2 films, were calculated from thicknesses measured by reflectometer divided by the number of growth cycles. For the nanolaminate, the GPC values were calculated from sublayer thicknesses measured by XRR divided by the number of growth cycles in the sublayer. Some of the Al_2O_3, ATO, and TiO_2 characterization results were published already in Refs. 53 and 54.

		Growth cycles								TOF-ERDA chemical composition (atm. %)							
		NL super cycles				Growth per cycle (nm)											
ALD film	Growth temperature (°C)		Al_2O_3	TiO_2	Al_2O_3 cap	Al_2O_3	TiO_2	Refractive index	XRR density (g/cm^3)	H	C	Cl	O	Al	Ti	GIXRD	Source
Al_2O_3	110	—	1283	—	—	0.0732	—	1.615	2.85	11.3	0.94	—	53.9	33.9	—	—	53
	150	—	1137	—	—	0.0841	—	1.638	2.95	5.6	0.50	—	58.1	35.8	—	—	53
	200	—	1037	—	—	0.0928	—	1.649	3.05	2.5	0.24	—	58.2	39.0	—	—	53
	250	—	1037	—	—	0.0936	—	1.655	3.10	1.4	0.15	—	60.0	38.4	—	—	53
	300	—	1109	—	—	0.0897	—	1.657	3.10	1.0	0.18	—	59.6	39.2	—	—	53
ATO	110	20	26	58	26	0.0785	0.0500	2.106	3.36	4.7	0.25	1.00	61	13	20	—	This work
	150	20	23	69	23	0.0913	0.0429	2.160	3.40	2.2	0.15	0.70	62	14	22	—	This work
	200	20	21	74	21	0.0881	0.0405	2.181	3.53	1.0	0.12	0.30	63	14	22	—	This work
	250	20	21	59	21	0.0905	0.0373	2.125	3.54	0.5	0.14	0.07	62	18	19	—	This work
	300	20	22	64	22	0.0909	0.0328	2.135	3.46	0.3	0.07	0.03	62	18	19	—	This work
TiO_2	110	—	—	1924	—	—	0.0509	2.417	3.70	1.0	0.20	1.90	65	—	32	—	54
	150	—	—	2313	—	—	0.0429	2.452	3.75	0.3	<0.10	0.80	65	—	34	—	This work
	200	—	—	2467	—	—	0.0408	2.603	3.80	0.2	<0.10	0.34	66	—	34	Anatase	54
	250	—	—	1953	—	—	0.0522	2.585	3.75	0.2	0.19	<0.05	66	—	33	Anatase	This work
	300	—	—	2124	—	—	0.0497	2.731	3.85	<0.05	<0.05	<0.05	67	—	33	Anatase	54

TABLE II. Thin film characterization results for ATO nanolaminates as a function of the (1) ALD temperature, (2) TiO_2 fraction, (3) bilayer thickness, and (4) total nanolaminate thickness. Some of the characterization results from series (3) bilayer thickness were published already in Ref. 14. Some ATO temperature series results, presented already in Table I, are repeated here for completeness.

		Growth cycles				Reflectometry, 5 pts					XRR thickness (nm)		XRR density (g/cm^3)		XRR roughness (nm)		Growth per cycle (nm)		GIXRD
Varied parameter	Growth temperature (°C)	NL cyc			Al_2O_3 cap	Thickness (nm)	St. dev (nm)	St. dev. (%)	Refractive index —	St. dev. —									observed peaks
			Al_2O_3 cyc	TiO_2 cyc							Al_2O_3	TiO_2	Al_2O_3	TiO_2	Al_2O_3	TiO_2	Al_2O_3[a]	TiO_2[a]	
(1) ALD temperature	110	20	26	58	26	99.5	2.0	2.0	2.106	0.008	2.04	2.90	2.80	3.60	0.5	0.5	0.0785	0.0500	—
	150	20	23	69	23	100.3	2.0	2.0	2.160	0.008	2.20	2.86	2.90	3.80	0.1	0.1	0.0913	0.0429	—
	200	20	21	74	21	93.4	1.9	2.0	2.181	0.007	2.15	2.74	2.95	3.80	0.3	0.6	0.0881	0.0405	—
	250	20	21	59	21	77.0	1.1	1.4	2.125	0.004	1.70	2.40	3.00	3.85	0.1	0.1	0.0905	0.0373	—
	300	20	22	64	22	72.9	0.8	1.1	2.135	0.003	1.7	2.40	3.10	3.85	0.1	0.1	0.0909	0.0328	—
(2) TiO_2 fraction	200	0	1040	0	21	97.9	1.8	1.8	1.643	0.002	98.00	—	3.00	—	0.6	—	0.0942	—	—
	200	20	41	25	21	92.8	1.8	1.9	1.853	0.003	3.89	0.85	2.95	3.90	0.3	0.5	0.0910	0.0400	—
	200	20	31	49	21	92.5	1.9	2.1	2.015	0.005	2.95	1.88	2.90	3.80	0.3	0.7	0.0903	0.0402	—
	200	20	21	74	21	93.4	1.9	2.0	2.181	0.007	2.15	2.74	2.95	3.80	0.3	0.6	0.0881	0.0405	—
	200	20	10	99	21	92.6	2.2	2.4	2.346	0.008	0.95	3.90	2.95	3.80	0.1	0.5	0.0850	0.0404	—
	200	0	0	2467	21	100.0	2.5	2.5	2.522	0.016	—	98.50	—	3.70	—	1.4	—	0.0399	(101)
(3) Bilayer thickness	200[b]	1000	1	1	21	128.9	2.5	1.9	1.965	0.004	138.5		3.35		0.9		0.0685		—
	200[b]	400	1	3	21	83.1	1.4	1.7	2.231	0.003	94.0		3.70		0.9		0.0580		—
	200[b]	200	3	6	21	99.9	1.4	1.4	2.118	0.004	110.5		3.60		0.8		0.0607		—
	200	133	4	9	21	89.5	1.8	1.9	—	—	0.38	0.38	3.05	3.90	—	0.3	0.0950	0.0422	—
	200	100	5	12	21	90.6	1.4	1.5	2.134	0.004	0.49	0.48	3.10	4.00	—	0.3	0.0980	0.0400	—
	200	50	10	25	21	90.5	1.4	1.5	2.129	0.004	1.00	0.93	2.90	3.90	—	0.8	0.1000	0.0372	—
	200	20	26	62	21	93.9	1.6	1.7	2.097	0.006	2.40	2.45	3.10	3.90	—	0.6	0.0885	0.0411	—
	200	10	52	123	21	96.4	1.7	1.8	2.091	0.006	5.25	4.50	2.95	3.75	—	0.8	0.0904	0.0407	—
	200	5	104	247	21	98.9	1.6	1.6	2.092	0.007	9.75	9.65	2.95	3.75	0.5	0.8	0.0913	0.0401	—
	200	2	259	617	21	104.2	1.7	1.6	2.110	0.008	23.70	24.50	2.95	3.80	0.5	0.8	0.0915	0.0397	—
	200	1	519	1233	21	—	—	—	—	—	50.00	48.30	2.95	3.75	0.5	0.8			(101), (004), (200), (105)
(4) Total thickness	200	4	21	74	21	—	—	—	—	—	1.90	3.10	3.80	3.80	0.3	0.3	0.0905	0.0419	—
	200	10	21	74	21	48.9	1.2	2.5	2.154	0.010	2.10	2.90	3.00	3.70	0.3	0.3	0.1000	0.0392	—
	200	20	21	74	21	93.4	1.9	2.0	2.181	0.007	2.15	2.74	2.95	3.80	0.3	0.6	0.0881	0.0405	—
	200	60	21	74	21	278.4	5.0	1.8	2.197	0.008	1.90	2.95	3.10	3.80	0.3	0.3	0.0905	0.0399	—

[a]GPC calculated from the XRR sublayer thickness divided by the number of growth cycles.
[b]Mixed oxide.

nanolaminate contained less TiO_2 at higher temperatures than expected, resulting in a lower refractive index.

The Al_2O_3 and TiO_2 sublayer densities presented in Table II were in line with the density values measured for the reference Al_2O_3 (Ref. 53) and TiO_2 (Ref. 54) samples. The total nanolaminate density had a local maximum around 250 °C, presented in Table I.

An approximately constant TiO_2 fraction around 60% was measured for nanolaminates grown at ALD temperatures from 110 to 200 °C. TiO_2 fraction dropped to around 50% at higher temperatures, which differs from the targeted 60%. Titanium and TiO_2 concentrations calculated from TOF-ERDA and XRR results were in line as presented in Fig. 2(a). The impurity concentrations decreased with increasing growth temperature as presented in Table I. The hydrogen content was 4.7 at. % at 110 °C and decreased to 0.3 at. % at 300 °C. The carbon levels were less than 0.3-at. % at 110 °C and decreased further with increasing ALD temperature. The chlorine levels, measured with RBS, decreased from 1 at. % for film grown at 110 °C to 0.03 at. % at 300 °C. The impurity levels of the nanolaminates were somewhat lower than expected on basis of the rule of mixture, as presented in Fig. 3(a).

As no crystalline peaks were observed with GIXRD, the nanolaminates were concluded to be amorphous through the

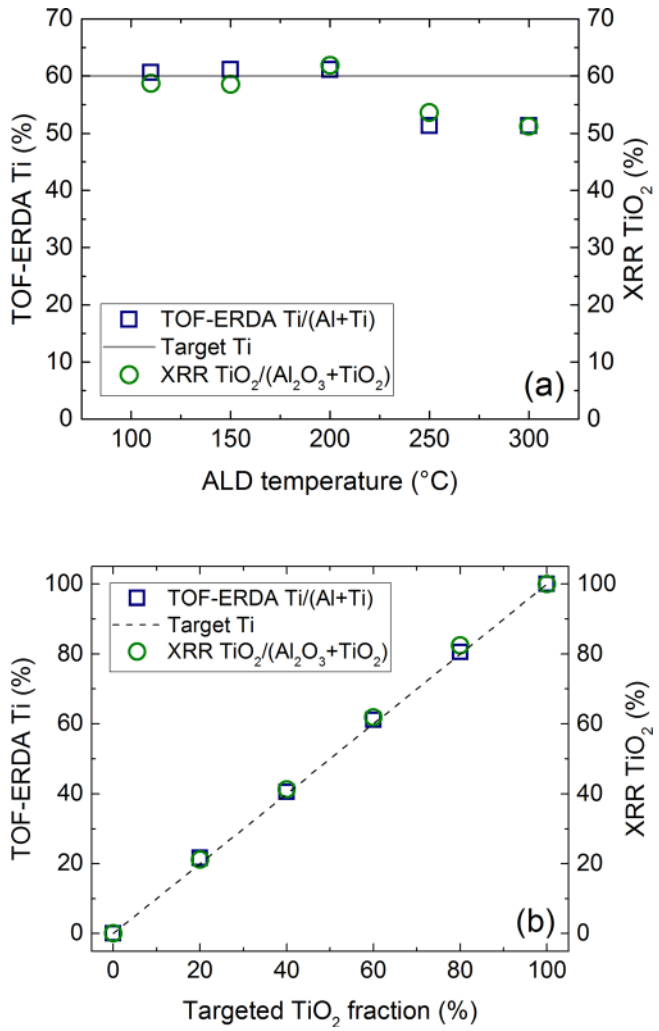

FIG. 2. (Color online) Ti and TiO_2 concentrations measured with TOF-ERDA and XRR, respectively, as a function of the (a) ALD temperature and (b) TiO_2 fraction.

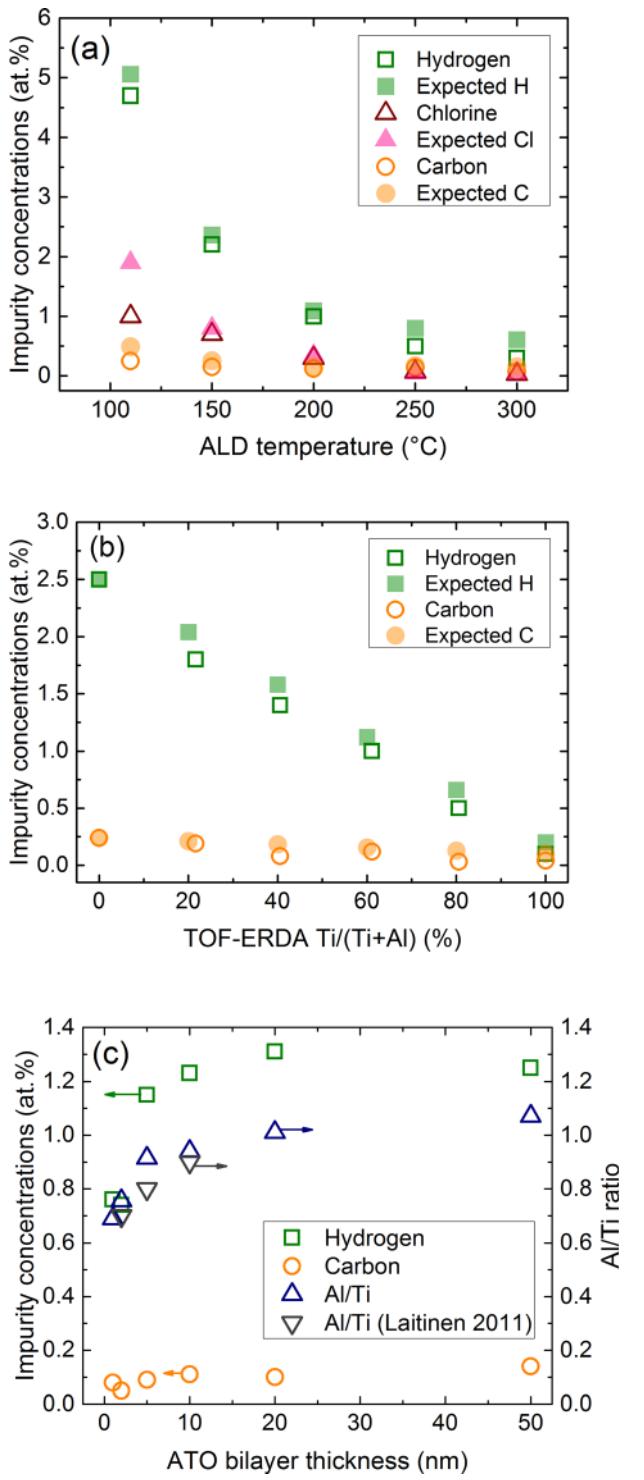

FIG. 3. (Color online) Impurity concentrations measured with TOF-ERDA and RBS (Cl) for ATO nanolaminates presented as a function of (a) ALD temperature, while keeping the total thickness, bilayer thickness, and TiO_2 fraction constant, and (b) TiO_2 fraction, while ALD temperature, total nanolaminate, and bilayer thickness were kept constant, and (c) ALD bilayer thickness. The expected impurity concentrations were calculated from the impurity values of the reference ALD Al_2O_3 and TiO_2 films using the rule of mixture.

ALD temperature range (Table I). The reference ALD Al_2O_3 was amorphous[53] while the reference TiO_2 (Ref. 54) had amorphous structure for films grown at 110 to 150 °C and at higher ALD temperatures polycrystalline structure with anatase phase.

2. ATO TiO_2 fraction series

TiO_2 fraction was varied from 0% to 100%, while the growth temperature, and the bilayer and the total thicknesses were kept constant at 200 °C, and 5 nm and 100 nm, respectively. The measurement results are presented in Table II.

GPC values were approximately constant for the TiO_2 sublayer with increasing TiO_2 fraction and were close to the GPC of the reference TiO_2 film grown at 200 °C. For the Al_2O_3 sublayer, the GPC decreased with increasing TiO_2 fraction. The refractive index increased linearly with increasing TiO_2 fraction and it had linear correlation with density values (calculated from the XRR results), as expected. According to XRR, the nanolaminate sublayers were smoother than reference Al_2O_3 and TiO_2 samples, with roughness of about 0.3 and 0.6 nm for Al_2O_3 and TiO_2 sublayers, respectively. The reference TiO_2 had XRR roughness of 1.4 nm (polycrystalline), while the reference Al_2O_3 had 0.6 nm roughness.

The Ti and TiO_2 fraction, calculated both from TOF-ERDA and XRR measurements, respectively, were in accordance with target TiO_2 values presented in Fig. 2(b). The hydrogen content decreased from 2.5 to 0.1 at. % with increasing TiO_2 content, as shown in Fig. 3(b). A similar behavior was observed with carbon, which decreased from 0.24 to 0.04 at. %. The hydrogen level was lower than detected for the reference Al_2O_3. The Cl content was not analyzed for the TiO_2 fraction series.

3. ATO nanolaminate bilayer thickness series

The nominal bilayer thickness in the nanolaminate was increased from about 0.1 to 100 nm while the total target thickness and the ALD temperature were kept constant at 100 nm and 200 °C, respectively. The target TiO_2 fraction was 50 vol. %. The characterization results are presented in Table II. Discrete sublayers were detected in the nanolaminate with the bilayer thickness down to 0.8 nm as analyzed earlier,[14] while the structures with nominal bilayer thickness less than 0.8 nm were in practice mixed oxides. The sample with the bilayer thickness of 100 nm was the only sample where the polycrystalline structure with the anatase phase was detected by GIXRD, and the other samples were amorphous.

The TiO_2 fraction was approximately constant measured both with XRR (Ref. 14) and TOF-ERDA with increasing bilayer thickness. For samples with bilayer thicknesses less than 1 nm, the targeted TiO_2 fraction of 50 vol. % was not achieved, because the amount of material grown by a single cycle could not be continuously tuned. Nanolaminates with thinnest bilayers had lowest impurity content [Fig. 3(c)]. The hydrogen content correlated with the Al content in the film.

4. ATO nanolaminate thickness series

The total nanolaminate thickness was varied from 20 to 300 nm while the bilayer thickness, the TiO_2 fraction and the ALD temperature were kept constant at 5 nm, 60%, and 200 °C. The results are presented in Table II. The nanolaminate thickness increased linearly with the number of nanolaminate supercycles. The refractive index and the density of Al_2O_3 and TiO_2 sublayers were approximately constant. All samples were amorphous.

B. Residual stress

The residual stress of ATO nanolaminate decreased from about 470 to 360 MPa with increasing ALD temperature as presented in Fig. 4(a) and Table III. For comparison, the stress results are also presented for the reference Al_2O_3 from Ref. 53 and the TiO_2 samples as a function of the ALD temperature. In the reference TiO_2, the stress was constant up to 150 °C, after which an abrupt rise was measured and a stress maximum was achieved for samples grown at 200 °C. At higher temperature, the stress of TiO_2 decreased again. The TiO_2 results were in line with the corresponding sample

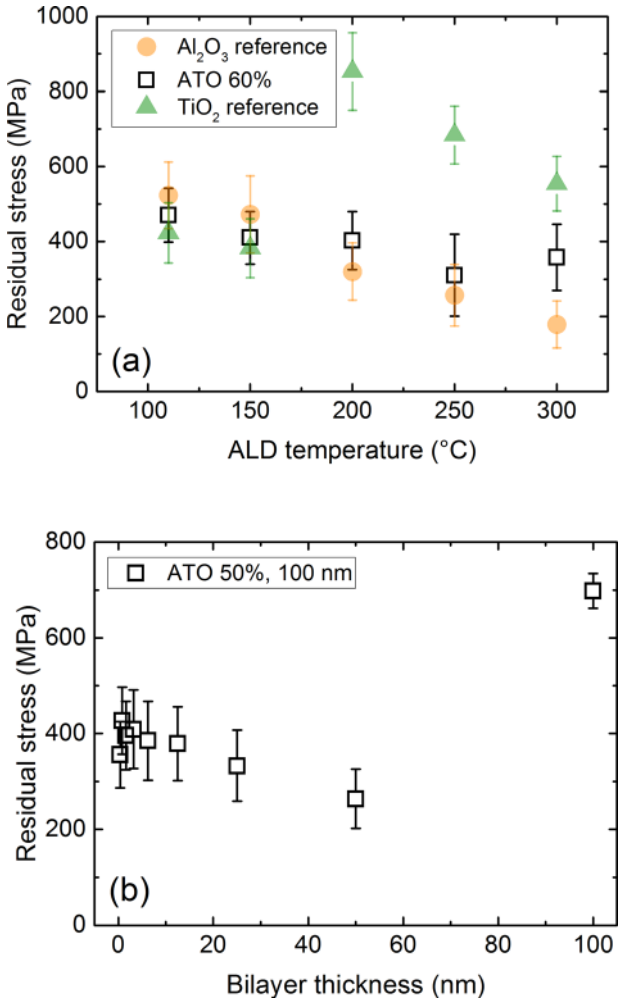

FIG. 4. (Color online) Residual stress of the ATO nanolaminate as a function of the (a) ALD temperature, and (b) bilayer thickness. The error bars present the maximum measurement uncertainty as explained in Sec. II.

TABLE III. Residual stress, contact modulus, hardness, and critical load values presented as a function of (1) ALD temperature, (2) TiO_2 fraction, (3) Bilayer thickness, and (4) Total nanolaminate thickness. Same values are also presented for reference ALD Al_2O_3, ALD TiO_2, and TAO nanolaminate grown at 200 °C. The residual stress results present average stress with maximum measurement uncertainty. The contact modulus and hardness values present the average of 15 measurements with standard deviation. The critical load values present the average of three measurements with standard deviation. Some of the Al_2O_3 and TiO_2 results were from Ref. 50.

	ALD temperature (°C)	TiO_2 fraction (%)	Total XRR thickness (nm)	Bilayer thickness (nm)	Residual stress (MPa)	Contact modulus (GPa)	Hardness (GPa)	L_{CSi1} (mN)	L_{CSi2} (mN)	L_{CALD1} (mN)	L_{CALD2} (mN)
Silicon reference	—	—	—	—	—	147	9.4	580 ± 20	610 ± 15	—	—
(1) ALD temperature	110[a]	60	98.9	5.0	470 ± 80	146 ± 6	6.9 ± 0.0	—	859 ± 7	1018 ± 60	1140 ± 110
	150[a]	60	101.2	5.0	410 ± 70	145 ± 3	7.5 ± 0.1	—	845 ± 7	1065 ± 40	1202 ± 35
	200[a]	60	97.8	5.0	400 ± 80	146 ± 9	7.5 ± 0.0	—	810 ± 3	1013 ± 15	1089 ± 80
	250[a]	60	82.0	5.0	310 ± 110	156 ± 5	8.4 ± 0.1	—	756 ± 5	1018 ± 10	1187 ± 55
	300[a]	60	82.0	5.0	360 ± 90	152 ± 3	8.7 ± 0.1	—	773 ± 6	1002 ± 50	1170 ± 10
(2) TiO_2 fraction	200	20	92.8	5.0	320 ± 220	151 ± 7	8.4 ± 0.3	—	—	—	—
	200	40	92.5	5.0	340 ± 220	153 ± 3	8.0 ± 0.2	—	—	—	—
	200	60	93.4	5.0	320 ± 220	146 ± 9	7.5 ± 0.0	—	—	—	—
	200	80	93.6	5.0	340 ± 220	148 ± 3	7.1 ± 0.1	—	—	—	—
(3) Bilayer thickness	200	50	138.5	Mixed	400 ± 170	147 ± 1	8.0 ± 0.2	—	—	—	—
	200	50	94.0	Mixed	390 ± 240	153 ± 3	7.8 ± 0.1	—	—	—	—
	200[a]	50	92.0[b]	Mixed	360 ± 70	—	—	—	—	—	—
	200	50	110.5	Mixed	420 ± 210	153 ± 2	7.8 ± 0.1	—	—	—	—
	200[a]	50	89.9[b]	0.8	430 ± 70	—	—	—	—	—	—
	200	50	97.0	1.0	410 ± 230	152 ± 4	7.9 ± 0.0	—	—	—	—
	200[a]	50	87.9[b]	1.6	400 ± 70	—	—	—	—	—	—
	200	50	96.5	2.0	400 ± 220	145 ± 4	8.0 ± 0.1	—	—	—	—
	200[a]	50	90.1[b]	3.2	410 ± 80	—	—	—	—	—	—
	200	50	97.0	5.0	330 ± 220	151 ± 1	8.0 ± 0.0	—	—	—	—
	200[a]	50	89.5[b]	6.3	390 ± 80	—	—	—	—	—	—
	200	50	97.5	10.0	320 ± 210	155 ± 1	8.2 ± 0.2	—	—	—	—
	200[a]	50	95.4[b]	12.5	380 ± 80	—	—	—	—	—	—
	200	50	97.0	20.0	290 ± 200	151 ± 8	8.2 ± 0.2	—	—	—	—
	200[a]	50	94.6[b]	25.0	330 ± 70	—	—	—	—	—	—
	200[a]	50	99.9[b]	50.0	260 ± 60	—	—	—	—	—	—
	200[a]	50	96.4	50.0	270 ± 70	156 ± 6	7.9 ± 0.1	—	—	—	—
	200[a]	50	98.3	100.0	700 ± 40	—	—	—	—	—	—
(4) Total thickness	200[a]	60	20.0	5.0	530 ± 310	—	—	460 ± 90	668 ± 14	938 ± 54	1023 ± 20
	200[a]	60	50.0	5.0	420 ± 130	—	—	—	687 ± 25	1027 ± 75	1135 ± 50
	200[a]	60	117.8	5.0	380 ± 80	156 ± 9	7.5 ± 0.1	—	810 ± 3	1013 ± 15	1089 ± 80
	200[a]	60	291.0	5.0	320 ± 40	153 ± 7	7.9 ± 0.2	540 ± 140	1135 ± 7	1148 ± 7	1173 ± 10
Al_2O_3 reference	200	0	98.7	—	400 ± 210	156 ± 6	9.9 ± 0.3	—	817 ± 4	876 ± 60	1015 ± 20
TiO_2 reference	200	100	99.9	—	780 ± 230	151 ± 4	8.3 ± 0.9	626 ± 91	753 ± 17	987 ± 22	1001 ± 15
TAO	200[a]	60	91.1	5.0	350 ± 80	—	—	—	829 ± 5	918 ± 5	1110 ± 50

[a]For residual stress measurements, 380 ± 5 μm thick wafer was used.
[b]Film thickness measured with reflectometry.

series reported in Ref. 54. The increase in stress of TiO_2 coincides with transition to crystalline anatase.

An approximately constant residual stress was measured as a function of TiO_2 fraction for samples grown at 200 °C, as presented in Table III. The reference sample with 100% TiO_2 had substantially higher stress value compared to nanolaminates, due to the crystalline nature of the film.

Increasing the bilayer thickness from 0.8 to 50 nm, the residual stress decreased from 430 to 260 MPa, as shown in Fig. 4(b). An elevated stress of 700 ± 40 MPa was measured for the sample with the bilayer thickness of 100 nm, in line with change in film morphology (polycrystalline structure). The stress of mixed oxide samples (bilayer thickness <0.8 nm) was close to the stress value measured for the reference ALD Al_2O_3.

The residual stress values as a function of film thickness, from 50 to 300 nm, were within measurement accuracy of this work, and thus, no conclusions can be made on the basis of the results, as presented in Table III.

Upon thermal cycling from room temperature up to 500 °C, of about 100 nm thick, 60% ATO nanolaminate grown at 300 °C, minor stress relaxation was measured. When annealing temperature reached the growth temperature, some amount of tensile residual stress (about 100 MPa) was measured, indicating that besides thermal stress there is growth related stress in the film. At annealing temperatures above 400 °C, compressive stress was measured in the stress–temperature curve as presented in Fig. 5; this was because of the thermal mismatch between the silicon substrate and the ALD film. As the stress–temperature curve was reversible with little hysteresis and only minor stress relaxation was measured for room temperature values, we conclude that no phase changes occurred during the thermal cycling and the morphological properties of the film were stable up to 500 °C.

C. Adhesion

Critical loads for the delamination of the ATO nanolaminates were measured as a function of the ALD temperature and the total nanolaminate thickness. The results were compared to the values of reference silicon substrate, ALD Al_2O_3 (Refs. 53 and 50) and ALD TiO_2 (Ref. 50) films, and nanolaminate starting with a TiO_2 layer (TAO). The numerical results are presented in Table III.

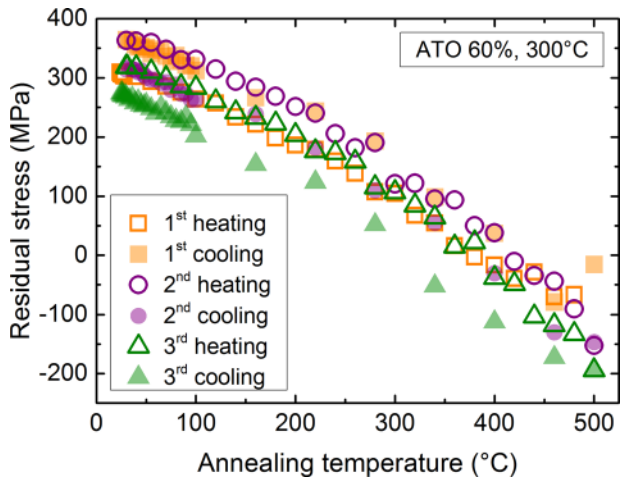

FIG. 5. (Color online) Residual stress as a function of thermal cycling temperature from room temperature up to 500 °C.

For the reference silicon without coating, the first initial failure (L_{CSi1}) and continuous breakage (L_{CSi2}) occurred at critical loads slightly before and close to 600 mN, respectively. The presence of ALD films increased the critical load value L_{CSi2}.

For all ATO films as well as reference ALD films, delamination of the film occurred after breakage of the silicon substrate ($L_{CALD1} > L_{CSi2}$). This indicates a strong adhesion between the nanolaminate and the silicon in all cases. Overall, the critical load values (L_{CALD1} and L_{CALD2}) representing the adhesion performance of the ATO films were at a similar high level as of reference ALD Al_2O_3 and TiO_2 (grown at 200 °C). The only exception was the ATO film with a total thickness of 20 nm, which had the overall lower critical load values compared to other films. The growth temperatures up to 200 °C provided similar critical load values L_{CSi2}, but the ATO nanolaminates grown at temperatures from 250 to 300 °C showed slightly lower critical load values.

No significant difference was found between the critical load values or the delamination behavior of TAO when compared to the ATO laminate (both grown at 200 °C, TiO_2 fraction 60%, and total thickness 100 nm).

D. Contact modulus and hardness

The nanoindentation hardness and contact modulus values are presented in Table III. The values represent an average of 15 indents performed under displacement control (indent depth 40–80 nm). Since the Poisson's ratio of the laminate was not precisely known, the contact modulus instead of elastic modulus is given. The contact modulus represents the combined elastic response of the specimen, indenter, and the load-frame of the instrument, and is related to the elastic modulus of the specimen through the Poisson's ratio of both the specimen and the indenter, as well as the elastic modulus of the indenter.

The elastic behavior of the laminate remained approximately constant, independent of the TiO_2 fraction, bilayer thickness, or ALD temperature. The highest hardness values were measured for the lowest TiO_2 fraction and at highest ALD temperature, at 300 °C, while the hardness remained nearly constant with increasing bilayer thickness.

IV. DISCUSSION

A. Short literature review

This work concerns ATO nanolaminates consisting of sublayers grown with the Me_3Al/H_2O and $TiCl_4/H_2O$ processes. The Me_3Al/H_2O was first reported in the late 1980s.[58] The Me_3Al/H_2O process to grow Al_2O_3 is, because of its near-ideal nature, sometimes considered a "model" for ALD,[3,6,59,60] and it might be the most widely used ALD process. A dedicated review article has been written on its

reaction mechanisms,[61] and the reaction mechanisms are further discussed in our recent publications.[53,62]

The $TiCl_4/H_2O$ has been known over 45 years, and it may even be the oldest ALD process known[63,64] and the second-most widely used ALD process. A dedicated review has been written about the reaction mechanisms and "agglomeration phenomenon" in this process, taking place beyond 300 °C.[65]

Taking into account the widespread use of these two processes, there is surprisingly little information available on combining these two processes as ATO. ATO has been used industrially since the 1980s in electroluminescent displays;[66] however for that, chloride reactant is also used for the Al_2O_3 component. The first report of ATO films by combining the Me_3Al and $TiCl_4$-based processes is from year 1999 (Ref. 42) and several studies have been made thereafter.[20,25,67,68] At VTT, the ATO process was taken in use in mid-2000 s. The overall reaction equations are

$$2Me_3Al\,(g) + 3H_2O\,(g) \rightarrow Al_2O_3(s) + 6CH_4(g),$$

$$TiCl_4(g) + 2H_2O\,(g) \rightarrow TiO_2(s) + 4HCl\,(g).$$

Interesting findings have been made regarding combining the Me_3Al/H_2O and $TiCl_4/H_2O$ ALD processes as ATO nanolaminates or mixed oxides. From TOF-ERDA results, Laitinen *et al.*[69] has reported a smaller Al/Ti ratio with decreasing bilayer thickness (down to 2 nm). The change in Al/Ti-ratio was proposed to be either due to enhanced GPC (called growth rate in Ref. 70) of TiO_2, reduced GPC of Al_2O_3 during the first cycles, or etching of Al_2O_3 by $TiCl_4$. Sintonen *et al.*,[14] on the basis of extended XRR measurements for the same sample series as in this work, reported that down to a bilayer thickness of about 0.8 nm (nominal thickness of 0.4 nm for both constituent oxides), the structure remains a laminate that consists of two distinctive and separate layers. Both amorphous and crystalline ALD TiO_2 sublayers have been reported for ATO nanolaminates depending on the TiO_2 thickness, ALD temperature, and substrate.[39,68,70,71]

B. ALD growth

The GPC of the TiO_2 sublayer in the ATO films had a different trend with temperature than the GPC in thicker pure TiO_2 films, as shown in Table I. It has been observed that the GPC in the $TiCl_4/H_2O$ process decreases with temperature, then increases, and goes through a maximum, after which it decreases again.[72] The increase in GPC occurs at the same time with crystallization.[73] For the TiO_2 sublayer in the ATO films, no intermediate increase was observed; instead, there was a continuously decreasing trend. The thin TiO_2 sublayer films in ATO remained amorphous up to 300 °C (Table I), so the difference in GPC of TiO_2 in ATO and TiO_2 as such is most likely related to differences in the film crystallinity. Because of the smaller GPC of TiO_2 in ATO than in thicker TiO_2 films used for reference, the resulting TiO_2 contents in the films deposited at >200 °C were less than expected, roughly 50 vol. % instead of the targeted 60 vol. %.

The ATO films were, throughout the temperature range used in this work (110–300 °C), somewhat purer than expected on the basis of the impurities in thicker Al_2O_3 and TiO_2 films (calculated using the rule of mixture). At 110 °C, chlorine content was significantly lower than expected from the impurity content of the reference oxides. Hydrogen content was lower throughout the temperature range used. The sources of carbon and chlorine are the Me_3Al and $TiCl_4$ reactants, respectively. The hydrogen originates mostly from the H_2O precursor.[62] The interfaces between Al_2O_3 and TiO_2 seem to have lower impurity contents (Cl, C, and H) than the bulk materials.

From the results obtained for the TiO_2 fraction series and ATO bilayer thickness series (both at 200 °C), one can estimate how Al_2O_3 grows on TiO_2. The average GPC of Al_2O_3 and TiO_2 on a TiO_2 starting surface (data in Table II) is plotted in Fig. 6 for the two series for the conditions a laminate is grown. Overall, it is seen that the average GPC of Al_2O_3 is lower in the beginning of the growth and increases toward a steady value of 0.092–0.094 nm. The two series in general agree, with the exception of the first three points of the ATO bilayer series, which give a significantly higher GPC of Al_2O_3. Generalizing the main result, the GPC of Al_2O_3 is

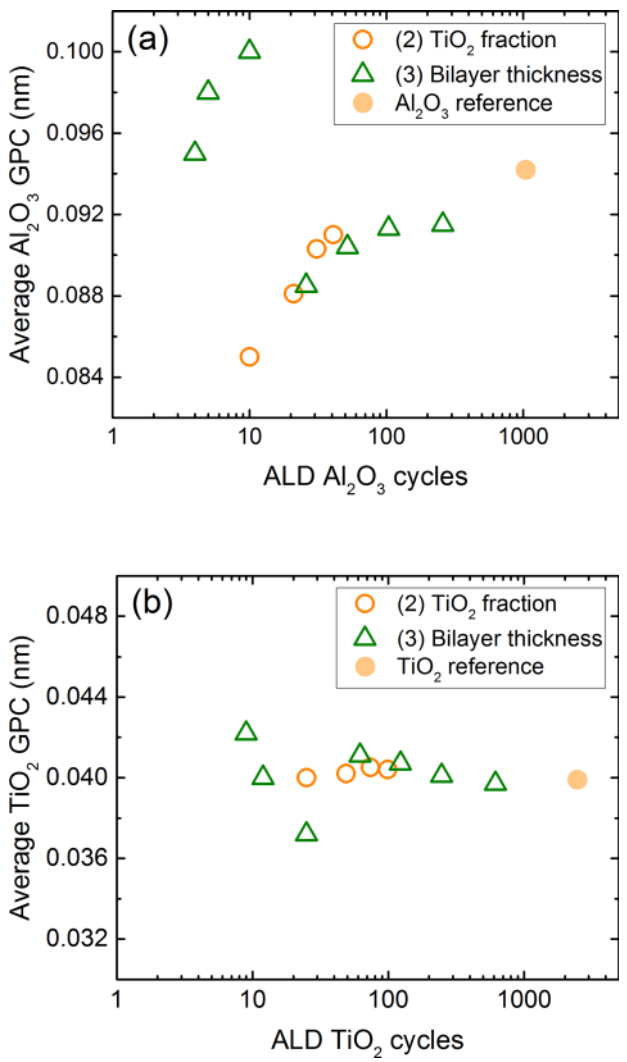

FIG. 6. (Color online) Average GPC for (a) Al_2O_3 and (b) TiO_2 as a function of growth cycles.

thus smaller on TiO_2 than it is on itself. Such behavior has been classified as "substrate-inhibited growth of type 1."[3,74] It has been proposed that the GPC of the Me_3Al-H_2O process depends directly (but not with a 1:1 ratio but rather a 1:3 ratio) on the surface OH group density.[3,61] Our result therefore suggests that the OH group density at 200 °C on TiO_2 should be lower than it is on Al_2O_3. Comparison to literature supports the suggestion: for (polycrystalline) TiO_2, a density of 4.5 OH/nm^2 has been measured at 200 °C (Refs. 75 and 76) and for Al_2O_3, a significantly higher density of 7.1 OH/nm.[2,77] Regarding the first three points of the ATO bilayer thickness series where the GPC of Al_2O_3 was higher (4, 5, and 10 cycles of Al_2O_3 on very thin TiO_2 of 0.4–0.9 nm, Table II), the result differs from the series and is more difficult to explain. While the reason for the higher GPC of Al_2O_3 remains unknown at the moment, we speculate that, in that case, the very thin TiO_2 layer may differ in character as compared to thicker, more bulklike, continuous TiO_2 layers, leading to different reaction mechanisms during the Me_3Al reaction and, as a result, a higher GPC. The unusually high density of TiO_2 measured for the thinnest layers by XRR (see Table II) is in accord with the special nature of the thinnest TiO_2 layers.

Similarly, as analyzed for Al_2O_3 on TiO_2, the results can also be used vice versa to analyze the growth of TiO_2 on Al_2O_3. On the basis of the results on Table II and Fig. 6, it seems that the GPC TiO_2 does not depend significantly on the cycles used. Therefore, TiO_2 ALD on Al_2O_3 follows the "linear growth" classification,[3,74] at least as long as TiO_2 remains amorphous. In the light of results, since Al_2O_3 has a smaller GPC on TiO_2 than it has on itself and the GPC of TiO_2 on Al_2O_3 was roughly the same as on TiO_2, it seems evident that from the mechanisms suggested by Laitinen *et al.*,[69] it is the "reduced growth rate" of Al_2O_3 that explains the lower Al/(Al+Ti) ratio in the beginning of ATO nanolaminate growth.

C. Residual stress

All ATO nanolaminates investigated in this work were under tensile residual stress. The residual stress of ATO decreased with increasing ALD temperature, from 470 MPa at 110 °C to 360 MPa at 300 °C. The TiO_2 fraction did not influence the residual stress of the nanolaminate (grown at 200 °C) as long as the sublayers remained amorphous. Our results are in line with those of Berdova *et al.*[49] for films grown at 220 °C (50% of TiO_2, 4 nm bilayer thickness, and residual stress ~450 MPa), and agree with the results of Behrendt *et al.*[48] for ATO films grown at 100 °C (50% of TiO_2, 2 nm bilayer thickness, and residual stress ~400 MPa) where residual stress was reported to be independent of the film thickness.

In the laminated structure with a constant overall composition (50% TiO_2), the residual stress decreased with increasing bilayer thickness as long as bilayers remained amorphous. Substantially higher stress was measured from the sample with a bilayer thickness of 100 nm due to a transition from amorphous to crystalline TiO_2. The transition occurs at a bilayer thickness greater than 50 nm. The tunability of the residual stress can be useful especially when the TiO_2 content and thus the refractive index in the nanolaminate need to be fixed.

For the mixed oxides with nominal bilayer thickness less than 0.8 nm, approximately a constant stress was measured (360 MPa). The maximum residual stress was measured for the sample with 0.8 nm bilayer thickness, in line with the observation that maximum tensile stress occurs when the film becomes completely continuous.[78] Our results are in line with the literature for mixed oxide grown at 220 °C.[49]

It is also interesting to compare our film stress results to earlier ATO nanolaminate film stress results. According to Maula *et al.*,[47] the stresses of TiO_2 and Al_2O_3, grown at 285 °C on an unknown substrate, were 190 MPa (tensile) and −65 MPa (compressive). (In our work, we use the convention that tensile stress is positive and compressive stress is negative in magnitude.) By stepwise incorporating more amorphous Al_2O_3 into the crystalline TiO_2, film stress could be diminished to approximately zero level (on the unknown substrate) at Al_2O_3/TiO_2 ratio of about 0.17. In our work, stress of 100 nm films of TiO_2 and Al_2O_3 grown at 200 °C were around 800 and 400 MPa, respectively, on silicon substrates. By incorporation of about 20% of Al_2O_3 in TiO_2, stress decreased significantly (by ~400 MPa), down to the level typical of the amorphous nanolaminates. It is likely that an accurate control of the Al_2O_3 fraction/sublayer thickness in more TiO_2-rich films would allow an accurate tuning of film stress in our case, too. Although the absolute stress values differed in our work compared to that of Maula *et al.*[47] (due to the use of different substrate materials) and we could not approach zero stress in this work, we conclude that the decreasing trend of tensile stress of TiO_2 with incorporation of Al_2O_3 was identical in the two works.

D. Adhesion

The amorphous ALD nanolaminate films had good adhesion properties on silicon, necessary to achieve the required functionality in MEMS structures. The ATO films were able to withstand similar critical loads before coating failure compared to the reference Al_2O_3 and TiO_2. This performance is in line with the earlier study of Kääriäinen *et al.*[51] on ALD Al_2O_3 and TiO_2 films.

The critical load values, determined in scratch testing for the silicon breakage and coating delamination, showed slightly increasing trend with the increasing coating thickness. However, the ATO film with an overall thickness of 20 nm had lower critical load values as compared to other films. The thinnest film also had the highest tensile residual stress, which might have reduced the critical loads, and thus influenced the adhesion performance of the coating.

The growth temperatures up to 200 °C provided equal critical load values. The ATO nanolaminates grown at temperatures from 250 to 300 °C showed slightly lower critical load values. This is related to the previously reported finding that the TiO_2 films grown at 250 °C and higher have lower critical loads in scratch testing than ALD Al_2O_3, behavior

most likely caused by crystallinity of the films grown in higher temperatures.[50]

No significant difference was found between the critical load values or the delamination behavior of TAO when compared to the ATO laminate (both grown at 200 °C, TiO_2 fraction 60%, and total thickness 100 nm). Therefore, both Al_2O_3 and TiO_2 can be used as the starting layers of ALD growth on RCA-cleaned silicon.

The presence of ALD nanolaminates postponed the breakage of the silicon and increased the critical load value L_{CSi2}. This suggests that the ALD nanolaminates increased the load carrying capacity of silicon, an observation also made for the single layer ALD films in an earlier work.[50]

E. Contact modulus and hardness

Contact modulus remained approximately constant; independent of the ALD temperature, TiO_2 fraction, and bilayer thickness. The laminate hardness depended linearly on the total TiO_2 fraction, the softer component in the laminate, as expected.

Varying the bilayer thickness, while keeping the TiO_2 fraction constant, caused no notable changes in the hardness. Our results are in close approximation to those in Ref. 39, where no significant changes in elastic modulus were detected with the increase in the bilayer thickness. Compared to the ZnO/Al_2O_3 laminate case by Raghavan *et al.*[37] and Homola *et al.*,[38] our case differs. Raghavan *et al.*[37] found that the laminates were the softer the thinner the bilayers, as the ZnO constituent layers in the nanolaminates simultaneously changed from crystalline to amorphous, in line with results of Homola *et al.*[38] In our case, the TiO_2 films were amorphous, and consequently, no changing trend was observed.

In the ATO temperature series, with the targeted constant composition of 60% TiO_2, the laminate hardness increased with the increase in the ALD temperature. This was unexpected, since previously published results for ALD Al_2O_3 (Ref. 53) have shown that the increase in hardness with the increase in temperature is marginal after 150 °C. Because of nonlinearity of the ALD ATO growth, the target and measured film composition differed at ALD temperatures above 200 °C, as the measured TiO_2 fraction was 50%. The amorphous TiO_2 is softer than the amorphous Al_2O_3; however, the crystalline TiO_2 is likely to be harder.[54] The tendency of TiO_2 grown on Al_2O_3 to crystallize increases, the higher the ALD temperature.[71] Although we did not observe crystalline TiO_2 in GIXRD, we consider it likely that the increase in hardness may originate from changes in the structure and nanocrystallinity of TiO_2.

V. CONCLUSIONS

Mixed oxides and nanolaminates were grown from Al_2O_3 and TiO_2 layers by ALD from $AlMe_3$, $TiCl_4$, and H_2O reactants. Fewer impurities were detected in ATO nanolaminates compared to the constituent oxide films. The nanolaminates were determined to be under tensile stress. The bilayer thickness and ALD temperature were the major parameters affecting the stress of the ATO layer. The residual stress increased with the decrease in the bilayer thickness and was independent of the TiO_2 content as long as the laminated structure remained amorphous. The stress decreased with the increase in growth temperature. The contact modulus was stable and independent of the growth temperature, TiO_2 fraction, and bilayer thickness. Higher growth temperatures provided harder ATO films. The nanolaminates with higher TiO_2 fraction were softer. The nanolaminates were able to withstand equal critical loads in scratch testing compared to the reference ALD Al_2O_3 and TiO_2 on silicon, and the nanolaminates also improved the load carrying capacity of the silicon. The adhesion of the ATO nanolaminates on silicon was good also regarding the functionality required in MEMS devices.

ACKNOWLEDGMENTS

This work has been carried out within the MECHALD project funded by Tekes and is linked to the Finnish Centres of Excellence in Atomic Layer Deposition (Reference No. 251220) and Nuclear and Accelerator Based Physics (Reference Nos. 213503 and 251353) of the Academy of Finland. Parts of these results were presented in oral presentation held at the 19th EuroCVD conference, September 1–6, 2013, Varna, Bulgaria, and at International Workshop on the Mechanical Behavior of Nanoscale Multilayers, October 1–4, 2013, Madrid, Spain.

[1]R. L. Puurunen, Chem. Vap. Deposition **20**, 332 (2014).
[2]A. A. Malygin, V. E. Drozd, A. A. Malkov, and V. M. Smirnov, Chem. Vap. Deposition **21**, 216 (2015).
[3]R. L. Puurunen, J. Appl. Phys. **97**, 121301 (2005).
[4]H. B. Profijt, S. E. Potts, M. C. M. van de Sanden, and W. M. M. Kessels, J. Vac. Sci. Technol., A **29**, 50801 (2011).
[5]V. Miikkulainen, M. Leskelä, M. Ritala, and R. L. Puurunen, J. Appl. Phys. **113**, 021301 (2013).
[6]S. M. George, Chem. Rev. **110**, 111 (2010).
[7]J. W. Elam, D. Routkevitch, P. P. Mardilovich, and S. M. George, Chem. Mater. **15**, 3507 (2003).
[8]F. Gao, S. Arpiainen, and R. L. Puurunen, J. Vac. Sci. Technol., A **33**, 10601 (2015).
[9]M. Ritala, M. Leskelä, L. Niinistö, T. Prohaska, G. Friedbacher, and M. Grasserbauer, Thin Solid Films **249**, 155 (1994).
[10]D. Riihelä, M. Ritala, R. Matero, and M. Leskelä, Thin Solid Films **289**, 250 (1996).
[11]M. Ritala, Appl. Surf. Sci. **112**, 223 (1997).
[12]J. W. Elam, Z. A. Sechrist, and S. M. George, Thin Solid Films **414**, 43 (2002).
[13]D. R. G. Mitchell, D. J. Attard, K. S. Finnie, G. Triani, C. J. Barbé, C. Depagne, and J. R. Bartlett, Appl. Surf. Sci. **243**, 265 (2005).
[14]S. Sintonen, S. Ali, O. M. E. Ylivaara, R. L. Puurunen, and H. Lipsanen, J. Vac. Sci. Technol., A **32**, 01A111 (2014).
[15]O. Sneh, R. B. Clark-Phelps, A. R. Londergan, J. Winkler, and T. E. Seidel, Thin Solid Films **402**, 248 (2002).
[16]S. V. Zhukovsky, A. Andryieuski, O. Takayama, E. Shkondin, R. Malureanu, F. Jensen, and A. V. Lavrinenko, Phys. Rev. Lett. **115**, 177402 (2015).
[17]J. I. Skarp, "Combination film, in particular for thin film electroluminescent structures," U.S. patent 4,486,487 (4 December 1984).
[18]T. Suntola and J. Hyvärinen, Annu. Rev. Mater. Sci. **15**, 177 (1985).
[19]A. Rissanen, U. Kantojärvi, M. Blomberg, J. Antila, and S. Eränen, Sens. Actuator, A **182**, 130 (2012).
[20]S. Zaitsu, T. Jitsuno, M. Nakatsuka, T. Yamanaka, and S. Motokoshi, Appl. Phys. Lett. **80**, 2442 (2002).
[21]N. Bilus Abaffy, D. G. McCulloch, J. G. Partridge, P. J. Evans, and G. Triani, J. Appl. Phys. **110**, 123514 (2011).

[22]N. Y. Garces, D. J. Meyer, V. D. Wheeler, Z. Liliental-Weber, D. K. Gaskill, and C. R. Eddy, J. Vac. Sci. Technol., B **32**, 03D101 (2014).
[23]A. P. Alekhin, A. A. Chouprik, S. A. Gudkova, A. M. Markeev, Y. Y. Lebedinskii, Y. A. Matveyev, and A. V. Zenkevich, J. Vac. Sci. Technol., B **29**, 01A302 (2011).
[24]P. F. Siles, M. de Pauli, C. C. Bof Bufon, S. O. Ferreira, J. Bettini, O. G. Schmidt, and A. Malachias, Nanotechnology **24**, 35702 (2013).
[25]I. Jõgi, K. Kukli, M. Kemell, M. Ritala, and M. Leskelä, J. Appl. Phys. **102**, 114114 (2007).
[26]G. Lee, B. K. Lai, C. Phatak, R. S. Katiyar, and O. Auciello, Appl. Phys. Lett. **102**, 142901 (2013).
[27]Y. S. Kim and S. Jin Yun, J. Cryst. Growth **274**, 585 (2005).
[28]P. C. Rowlette and C. A. Wolden, Thin Solid Films **518**, 3337 (2010).
[29]W. Li, O. Auciello, R. N. Premnath, and B. Kabius, Appl. Phys. Lett. **96**, 162907 (2010).
[30]W. Li, Z. Chen, R. N. Premnath, B. Kabius, and O. Auciello, J. Appl. Phys. **110**, 24106 (2011).
[31]G. Lee, B.-K. Lai, C. Phatak, R. S. Katiyar, and O. Auciello, J. Appl. Phys. **114**, 27001 (2013).
[32]I. Petrov, P. B. Barna, L. Hultman, and J. E. Greene, J. Vac. Sci. Technol., A **21**, S117 (2003).
[33]D. M. Hausmann and R. G. Gordon, J. Cryst. Growth **249**, 251 (2003).
[34]Z. A. Sechrist, F. H. Fabreguette, O. Heintz, T. M. Phung, D. C. Johnson, and S. M. George, Chem. Mater. **17**, 3475 (2005).
[35]A. Madan, Y. Wang, S. A. Barnett, C. Engstroüm, H. Ljungcrantz, L. Hultman, and M. Grimsditch, J. Appl. Phys. **84**, 776 (1998).
[36]M. Ben Daia, P. Aubert, S. Labdi, C. Sant, F. A. Sadi, P. Houdy, and J. L. Bozet, J. Appl. Phys. **87**, 7753 (2000).
[37]R. Raghavan, M. Bechelany, M. Parlinska, D. Frey, W. M. Mook, A. Beyer, J. Michler, and I. Utke, Appl. Phys. Lett. **100**, 191912 (2012).
[38]T. Homola, V. Buršíková, T. V. Ivanova, P. Souček, P. S. Maydannik, D. C. Cameron, and J. M. Lackner, Surf. Coat. Technol. **284**, 198 (2015).
[39]I. Iatsunskyi, E. Coy, R. Viter, G. Nowaczyk, M. Jancelewicz, I. Baleviciute, K. Załęski, and S. Jurga, J. Phys. Chem. C **119**, 20591 (2015).
[40]E. Marin, A. Lanzutti, M. Lekka, L. Guzman, W. Ensinger, and L. Fedrizzi, Surf. Coat. Technol. **211**, 84 (2012).
[41]E. Marin, L. Guzman, A. Lanzutti, W. Ensinger, and L. Fedrizzi, Thin Solid Films **522**, 283 (2012).
[42]R. Matero, M. Ritala, M. Leskelä, T. Salo, J. Aromaa, and O. Forsén, J. Phys. IV **9**, 493 (1999).
[43]E. Marin, A. Lanzutti, L. Guzman, and L. Fedrizzi, J. Coat. Technol. Res. **9**, 347 (2012).
[44]A. I. Abdulagatov, Y. Yan, J. R. Cooper, Y. Zhang, Z. M. Gibbs, A. S. Cavanagh, R. G. Yang, Y. C. Lee, and S. M. George, ACS Appl. Mater. Interfaces **3**, 4593 (2011).
[45]P. C. Yashar and W. D. Sproul, Vacuum **55**, 179 (1999).
[46]H. S. Chang, S. Jeon, H. Hwang, and D. W. Moon, Appl. Phys. Lett. **80**, 3385 (2002).
[47]J. Maula, K. Härkönen, and A. Nikolov, "Multilayer material and method of preparing same," U.S. patent 7,901,736 B2 (8 March 2011).
[48]A. Behrendt, J. Meyer, P. van de Weijer, T. Gahlmann, R. Heiderhoff, and T. Riedl, ACS Appl. Mater. Interfaces **8**, 4056 (2016).
[49]M. Berdova *et al.*, Acta Mater. **66**, 370 (2014).
[50]L. Kilpi, O. M. E. Ylivaara, A. Vaajoki, J. Malm, S. Sintonen, M. Tuominen, R. L. Puurunen, and H. Ronkainen, J. Vac. Sci. Technol., A **34**, 01A124 (2016).
[51]T. O. Kääriäinen, P. J. Kelly, D. C. Cameron, B. Beake, H. Li, P. M. Barker, and C. F. Struller, J. Vac. Sci. Technol., A **30**, 01A132 (2012).
[52]S. Ali, T. Juntunen, S. Sintonen, O. M. E. Ylivaara, R. L. Puurunen, H. Lipsanen, I. Tittonen, and S.-P. Hannula, Nanotechnology **27**, 445704 (2016).
[53]O. M. E. Ylivaara *et al.*, Thin Solid Films **552**, 124 (2014).
[54]J. Lyytinen *et al.*, Wear **342–343**, 270 (2015).
[55]R. L. Puurunen and H. Kattelus, "ALD ATO nanolaminates with adjustable electrical properties," in *ALD 2009, 9th International Conference on Atomic Layer Deposition*, Monterey, CA, 19–22 July (2009).
[56]M. Laitinen, M. Rossi, J. Julin, and T. Sajavaara, Nucl. Instrum. Methods Phys. Res., Sect. B **337**, 55 (2014).
[57]X. Liu, E. Haimi, S.-P. Hannula, O. M. E. Ylivaara, and R. L. Puurunen, J. Vac. Sci. Technol., A **32**, 01A116 (2014).
[58]G. S. Higashi and C. G. Fleming, Appl. Phys. Lett. **55**, 1963 (1989).
[59]K. Knapas and M. Ritala, Crit. Rev. Solid State Mater. Sci. **38**, 167 (2013).
[60]T. Weckman and K. Laasonen, Phys. Chem. Chem. Phys. **17**, 17322 (2015).
[61]R. L. Puurunen, Appl. Surf. Sci. **245**, 6 (2005).
[62]T. Sajavaara, J. Malm, J. Julin, M. Laitinen, K. Arstila, and R. L. Puurunen, "Origin of hydrogen impurity in Al_2O_3 thin films grown by ALD using Me_3Al and water (D_2O, H_2O) as precursors," in *AVS Topical Conference on Atomic Layer Deposition* (2014).
[63]S. I. Kol'tsov, J. Appl. Chem. USSR **42**, 975 (1969).
[64]A. M. Shevyakov, G. N. Kuznetsova, and V. B. Aleskovskii, "Interaction of titanium and germanium tetrachlorides with hydrated silica," in *Chemistry of High Temperature Materials. Proceedings of 2nd USSR Conference on High Temperature Chemistry of Oxides*, Leningrad, USSR, 26–29 November, 1965 (1967), pp. 162–168.
[65]R. L. Puurunen, Chem. Vap. Deposition **11**, 79 (2005).
[66]T. Suntola, J. Antson, A. Pakkala, and S. Lindfors, "Atomic layer epitaxy for producing EL-thin films," in *SID International Symposium on Digest of Technical Papers* (1980), pp. 108–109.
[67]S. I. Zaitsu, S. Motokoshi, T. Jitsuno, M. Nakatsuka, and T. Yamanaka, Jpn. J. Appl. Phys., Part 1 **41**, 160 (2002).
[68]D. R. G. Mitchell, G. Triani, D. J. Attard, K. S. Finnie, P. J. Evans, C. J. Barbé, and J. R. Bartlett, Smart Mater. Struct. **15**, S57 (2006).
[69]M. Laitinen *et al.*, Nucl. Instrum. Methods Phys. Res., Sect. B **269**, 3021 (2011).
[70]V. Fedorenko, I. Iatsunskyi, M. Pavlenko, M. Jancelewicz, E. Coy, and R. Viter, Proc. SPIE **9649**, 96490X (2015).
[71]R. L. Puurunen, T. Sajavaara, E. Santala, V. Miikkulainen, T. Saukkonen, M. Laitinen, and M. Leskelä, J. Nanosci. Nanotechnol. **11**, 8101 (2011).
[72]R. L. Puurunen, J. Saarilahti, and H. Kattelus, ECS Trans. **11**, 3 (2007).
[73]S. K. Kim, S. Hoffmann-Eifert, M. Reiners, and R. Waser, J. Electrochem. Soc. **158**, D6 (2011).
[74]R. L. Puurunen and W. Vandervorst, J. Appl. Phys. **96**, 7686 (2004).
[75]V. S. Lusvardi, M. A. Barteau, W. R. Dolinger, and W. E. Farneth, J. Phys. Chem. **100**, 18183 (1996).
[76]G. D. Parfitt, "The surface of titanium dioxide," in *Progress in Surface and Membrane Science*, edited by D. A. Cadenhead (Academic, New York, 1976), Vol. 11, pp. 181–226.
[77]R. L. Puurunen, M. Lindblad, A. Root, and A. O. I. Krause, Phys. Chem. Chem. Phys. **3**, 1093 (2001).
[78]M. F. Doerner and W. D. Nix, CRC Crit. Rev. Solid State Mater. Sci. **14**, 225 (1988).